PSFC/JA-14-25

# Core Impurity Transport in Alcator C-Mod L-, I- and H-mode Plasmas

Rice, J.E., Reinke[1], M.L., Gao, C., Howard, N.T., Chilenski, M.A., Delgado-Aparicio[2], L., Granetz, R.S., Greenwald, M.J., Hubbard, A.E., Hughes, J.W., Irby, J.H., Lin, Y., Marmar, E.S., Mumgaard, R.T., Scott[2], S.D., Terry, J.L., Walk, J.R., White, A.E., Whyte, D.G., Wolfe, S.M. and Wukitch, S.J.

[1]present address: University of York, York, UK
[2]Princeton Plasma Physics Laboratory, Princeton, NJ

December, 2014

**Plasma Science and Fusion Center**
**Massachusetts Institute of Technology**
**Cambridge MA 02139 USA**

This work was supported by the U.S. Department of Energy, Grant No.DE-FC02-99ER54512. 

**Core Impurity Transport in Alcator C-Mod L-, I- and H-mode Plasmas**

J.E. Rice, M.L. Reinke[†], C. Gao, N.T. Howard, M.A. Chilenski,
L. Delgado-Aparicio[♭], R.S. Granetz, M.J. Greenwald, A.E. Hubbard, J.W. Hughes,
J.H. Irby, Y. Lin, E.S. Marmar, R.T. Mumgaard, S.D. Scott[♭], J.L. Terry, J.R. Walk,
A.E. White, D.G. Whyte, S.M. Wolfe and S.J. Wukitch

*PSFC, MIT, Cambridge, Massachusetts 02139, USA*

[†]*University of York, York, YO10 5DD, UK*

[♭]*PPPL, Princeton, New Jersey 08543, USA*

**Abstract**

Core impurity transport has been investigated for a variety of confinement regimes in Alcator C-Mod plasmas from x-ray emission following injection of medium and high Z materials. In Ohmic L-mode discharges, impurity transport is anomalous ($D_{\rm eff} \gg D_{\rm nc}$) and changes very little across the LOC/SOC boundary. In ICRF heated L-mode plasmas, the core impurity confinement time decreases with increasing ICRF input power (and subsequent increasing electron temperature) and increases with plasma current. Nearly identical impurity confinement characteristics are observed in I-mode plasmas. In EDA H-mode discharges the core impurity confinement times are much longer. There is a strong connection between core impurity confinement time and the edge density gradient across all confinement regimes studied here. Deduced central impurity density profiles in stationary plasmas are generally flat, in spite of large amplitude sawtooth oscillations, and there is little evidence of impurity convection inside of r/a = 0.3 when averaged over sawteeth.

## I. Introduction

Understanding particle transport is essential for prediction of the density profile in ITER and other future reactor scale devices. In order to guide theory and simulation, direct observations of ion particle transport are necessary, but this is difficult in practice. A useful proxy is through the use of impurities, which are easy to inject and measure. Understanding impurity transport is important in its own right, since impurity accumulation can lead to ion dilution and radiative collapse. In the enhanced confinement operational regimes (H-mode and ITB plasmas) envisioned for future devices, long impurity confinement times are widely seen, with impurity transport approaching neo-classical levels in the barrier region [1, 2, 3, 4, 5, 6, 7, 8, 9, 10, 11, 12, 13, 14, 15, 16, 17, 18, 19, 20]. Since the neo-classical impurity density profile peaking factor increases strongly with atomic charge, H-mode and ITB plasmas in devices with tungsten (Z = 74) walls will potentially have a serious problem with tungsten accumulation and subsequent radiation. Further exacerbating this issue is the wall erosion due to ELMs associated with H-mode. Several experiments have indicated some relief from the core impurity accumulation problem using electron heating [14, 15, 17, 21, 22, 23, 24, 25, 26, 27]. In constrast, impurity related issues are not so serious in L-mode plasmas, which are long known to exhibit anomalous impurity transport [28, 29, 30, 31, 32, 10, 33, 34, 35, 36, 11, 37, 38, 39]. Recently there has been an emerging understanding of L-mode impurity transport through gyro-kinetic and fluid simulations [21, 17, 22, 40, 41, 42, 26, 43, 44, 27, 45, 46], including the effects of ITG modes and TEMs. A detailed study has been performed for C-Mod plasmas in the region $0.3 < r/a < 0.6$ [43, 44, 46]. Unfortunately, the energy confinement properties of L-mode are not currently attractive for reactor scenarios. An alternative is the I-mode regime [47, 48, 49, 50, 51, 52], which combines the good energy confinement of H-mode with the poor (yet favorable) particle and impurity confinement of L-mode.

In this paper the core impurity confinement properties of L-, I- and H-mode plasmas in Alcator C-Mod will be compared. Following a brief outline of the experimental setup in section II, including representative x-ray emissivity profiles, impurity transport in L-mode plasmas will be described in section III, presenting the results of scans of the electron density, auxiliary heating power, plasma current, toroidal magnetic field and background ion mass. In section IV impurity confinement in I-mode will be discussed, describing scans of plasma current and impurity mass, followed by a description of the dependence of impurity transport on plasma parameters in EDA H-mode discharges in section V. A general discussion and comparison of impurity transport in all operational regimes, and the relation to energy confinement and the edge density gradient, will be presented in section VI.

## II. Experimental Setup

This detailed study of core impurity transport has been performed on the Alcator C-Mod tokamak [53] (major radius R = 0.67 m, typical minor radius, $a$, of 0.21 m, with molybdenum plasma facing components). Operation was with both forward and

reversed magnetic field/plasma current, and in the upper single null (USN) and lower single null (LSN) configurations, mostly with deuterium working gas. Line averaged electron densities were in the range from 0.4 to $5.0\times10^{20}/m^3$, toroidal magnetic fields between 3.3 and 6.5 T and with plasma currents between 0.4 and 1.3 MA ($9 \leq q_{95} \leq 3$). Auxiliary heating was provided by ICRF waves (D(H) minority heating) [54] with power up to 4 MW. Current density profile modification can be achieved through use of lower hybrid range of frequencies (LHRF) waves [55] at 4.6 GHz, with total power up to 1.2 MW [54]. A set of corrections coils allows [56] for excitation of n = 1 magnetic perturbations which can be used to induce locked modes. Using these tools, C-Mod has access to the following confinement regimes: Ohmic L-mode with linear Ohmic confinement (LOC) and saturated Ohmic confinement (SOC), ICRF heated L-mode, I-mode [48], and enhanced $D_\alpha$ (EDA) [57] and ELM-free H-mode.

Electron densities were determined from a two color interferometer, fast electron temperature evolution using electron cyclotron emission (ECE) and $Z_{\rm eff}$ from visible *bremsstrahlung* [58]. Electron density and temperature profiles were provided by Thomson scattering [58]. Core toroidal rotation and ion temperature profiles were measured with an imaging x-ray spectrometer system [59, 60]. The impurities calcium (Z = 20, from $CaF_2$), molybdenum (Z = 42) and tungsten (Z = 74) were injected *via* a multi-pulse laser blow-off system [39]. Core impurity transport was characterized by spectroscopic measurement of subsequent x-ray emission from highly ionized He-like and H-like calcium ($Ca^{18+}$ and $Ca^{19+}$) [61] in addition to Ne-like molybdenum ($Mo^{32+}$) [36] and tungsten charge states near $W^{44+}$ [62]. The most intense calcium x-ray transitions observed are the $Ca^{19+}$ $Ly_\alpha$ doublet (1s $^1S_{1/2}$ - 2p $^2P_{3/2}$ at 3018.50 mÅ and 1s $^1S_{1/2}$ - 2p $^2P_{1/2}$ at 3023.92 mÅ) and the $Ca^{18+}$ resonance line w ($1s^2$ $^1S_0$ - 1s2p $^1P_1$ at 3177.26 mÅ) and forbidden line z ($1s^2$ $^1S_0$ - 1s2p $^3S_1$ at 3211.13 mÅ). In the core plasma, the upper levels of these transitions are populated predominantly by collisional excitation. A variety of x-ray instruments was utilized for observations of core impurity emission following injection: a single chord von Hamos type spectrometer [63] (time resolution 1 ms), the high resolution spatially imaging Johann type spectrometer system [59, 60] and a low energy resolution soft x-ray array [58]. For the imaging Johann spectrometers, typical time resolution is 20 ms, although it is possible operate at 6 ms (total acquisition plus readout time). Most of the discharges presented in this study exhibited sawtooth oscillations, with periods of order 10 ms, and most observations are sawtooth averaged.

Typical x-ray emissivity profiles are centrally peaked. The complete emissivity profile evolution for calcium lines is available from the x-ray imaging spectrometer system [59] following tomographic inversions [60]. An example of an emissivity profile for the resonance line w of $Ca^{18+}$ obtained at one time point during the impurity decay phase following an injection into a 5.4 T, 0.8 MA deuterium L-mode plasma with 1.3 MW of ICRF power ($<n_e>$ = $1.2\times10^{20}/m^3$, $q_{95}$ = 4.6) is shown in the top frame of Fig.1. Most of the emission is from inside of r/a = 0.5, which indicates that the central chord brightness reflects the impurity behavior in the core. Shown for comparison is the electron temperature profile from Thomson scattering (with fit). In the bottom frame is shown the electron density profile (and fit), which is slightly peaked. Also shown is the total calcium density, deduced from the w emissivity profile and

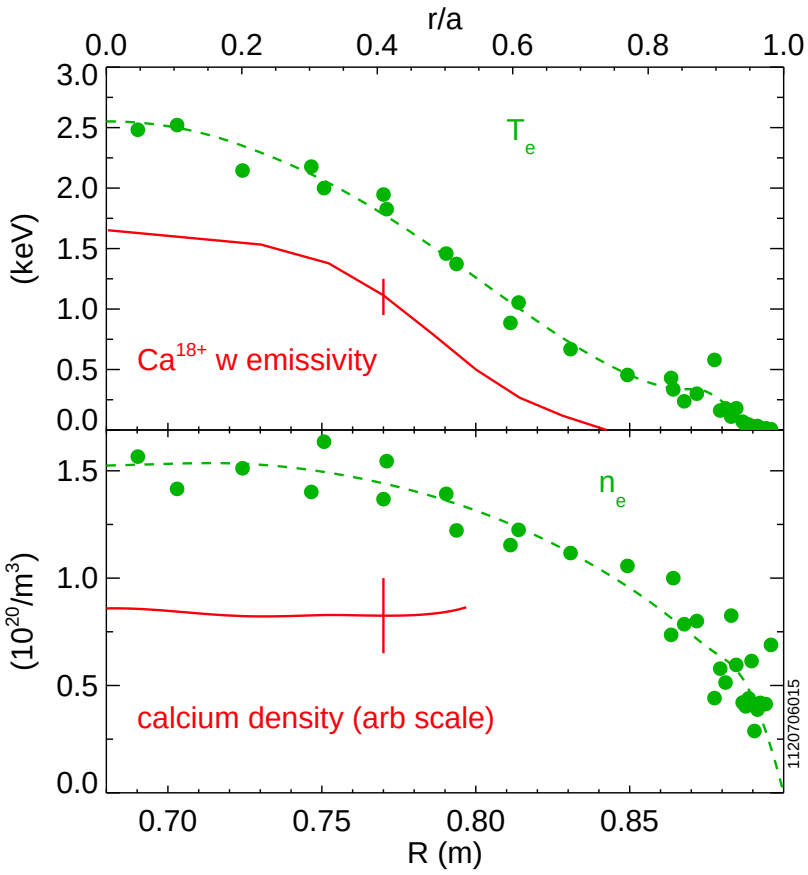


Figure 1: Profiles for a 5.4 T, 0.8 MA deuterium Ohmic L-mode plasma with $<n_e>$ = $1.2\times10^{20}$/m$^3$. Top frame: resonance line w ($Ca^{18+}$) emissivity profile (solid red) and electron temperature profile (green dots, with fit, green dashed line). Bottom frame: electron density profile (green dots, with fit, green dashed line) and relative total calcium density profile (solid red) at one particular time during the impurity decay following injection. The sawtooth inversion radius was R $\sim$ 0.77 m.

the upper level population model for He-like ions [64]. This assumes that individual charge states are in coronal equilibrium, and includes population of the upper level by collisional excitation and radiative recombination. This deduced calcium density profile is insensitive to sawtooth oscillations in this case since the excitation rate for the w line and the ionization rate for $Ca^{18+}$ have a similar electron temperature dependence; the ratio of these two rates changes by only 15% between 1.9 and 2.9 keV. The total calcium density in the core for this discharge is quite flat within the error bars, so there is no evidence for a particle pinch inside of r/a $\sim$ 0.5. Flat core calcium density profiles are also routinely observed in I- and H-mode plasmas when averaged over sawtooth oscillations. This justifies the use of an effective impurity diffusivity, $D_{\rm eff}$, derived from the long time scale impurity confinement time.

### III. L-mode

Impurity transport behavior and parameter scalings in L-mode plasmas will be explored in this section. Shown in Fig.2 are discharge time histories for a 5.4 T, 0.8 MA deuterium plasma with five $CaF_2$ injections, and five levels of ICRF D(H) minority heating power. This discharge was in the USN configuration with the ion $B\times\nabla B$ drift direction downward ('unfavorable') in order to prevent a transition into H-mode. Injection times were 0.565, 0.765, 0.965, 1.165 and 1.365 s, coinciding with 200 ms intervals of ICRF power in 1 MW steps. The first injection was into a purely Ohmic L-mode target with an average density of $1.0\times10^{20}/m^3$. At this density, with $q_{95}$ = 4.6, the plasma was in the satured Ohmic confinement (SOC) regime [65, 66, 67, 68], which is thought to be dominated by ITG mode turbulence. A global impurity confinement time, $\tau_I$, of 26 ms was deduced from the decay of the $Ca^{18+}$ signal (first injection, bottom frame) which corresponds to an effective diffusivity (ignoring convection and elongation) $D_{\rm eff} = a^2/(2.405)^2\tau_I \sim 0.29$ $m^2$/s, where $a$ is the plasma minor radius and 2.405 is the first zero of the zero order Bessel function. This is much larger than the core neo-classical diffusivity, $D_{\rm nc}$ ($\sim$ 0.02 $m^2$/s) [69, 7], so the impurity transport in L-mode is regarded as anomalous. Examination of the subsequent injections with increasing ICRF heating power (and electron temperature) reveals a systematic decrease in the core impurity confinement time. This is directly apparent from a comparison of $Ca^{18+}$ time histories as shown in Fig.3; the normalized brightnesses have been adjusted in time relative to each injection. The core impurity confinement time decreases systematically nearly a factor of two from 26 ms (fitted exponential decay shown) for the first injection to 14 ms for the fifth. $D_{\rm eff}$ correspondingly increases from 0.29 to 0.54 $m^2$/s. The results of the ICRF power scan for this discharge are summarized in Fig.4, showing $P_{\rm tot}$, which is the sum of the Ohmic and ICRF heating power. In the top frame is the core impurity confinement time, which decreases steadily with increasing total input power. Similar behavior has been observed in JET neutral beam heated L-mode plasmas [9]. Shown by the curves are the scalings derived for JET and Tore Supra [35] (dashed line proportional to ${P_{\rm tot}}^{-.57}$ at fixed density) and C-Mod [43] (solid line proportional to ${P_{\rm tot}}^{-.15}$). The observed power scaling for this one particular discharge seems to lie between the two curves. Other concomitant changes during this power scan

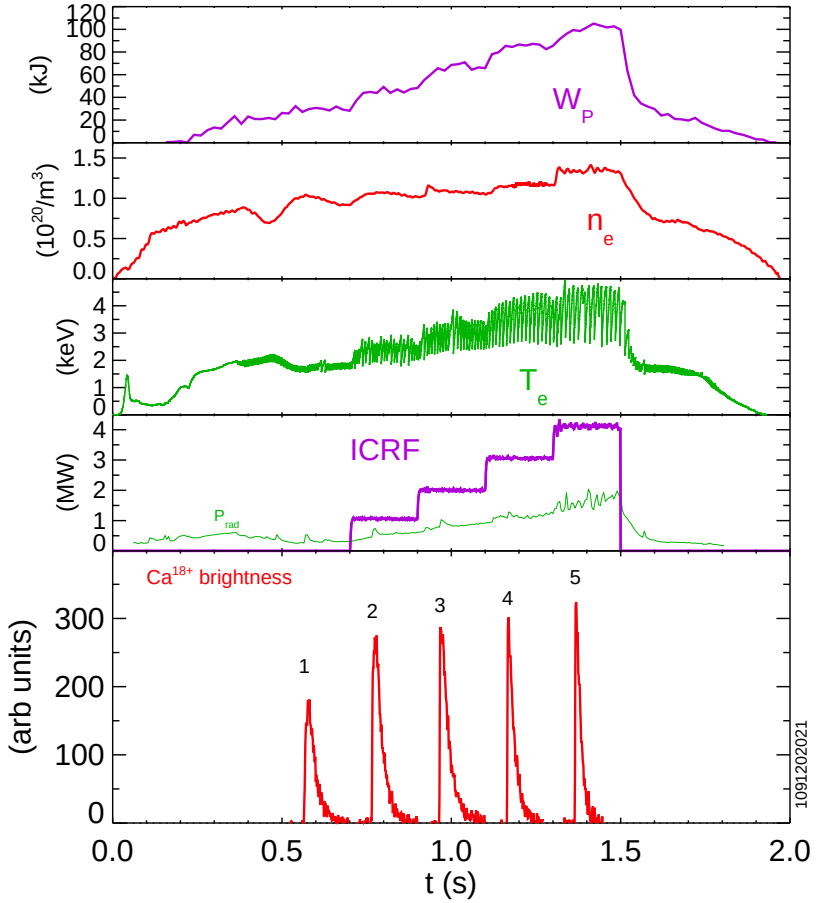


Figure 2: Parameter time histories for a 5.4 T, 0.8 MA deuterium discharge with five $CaF_2$ injections and five levels of ICRF power. From top to bottom, the plasma stored energy, average electron density, central electron temperature, ICRF power (and radiated power) and $Ca^{18+}$ brightness.

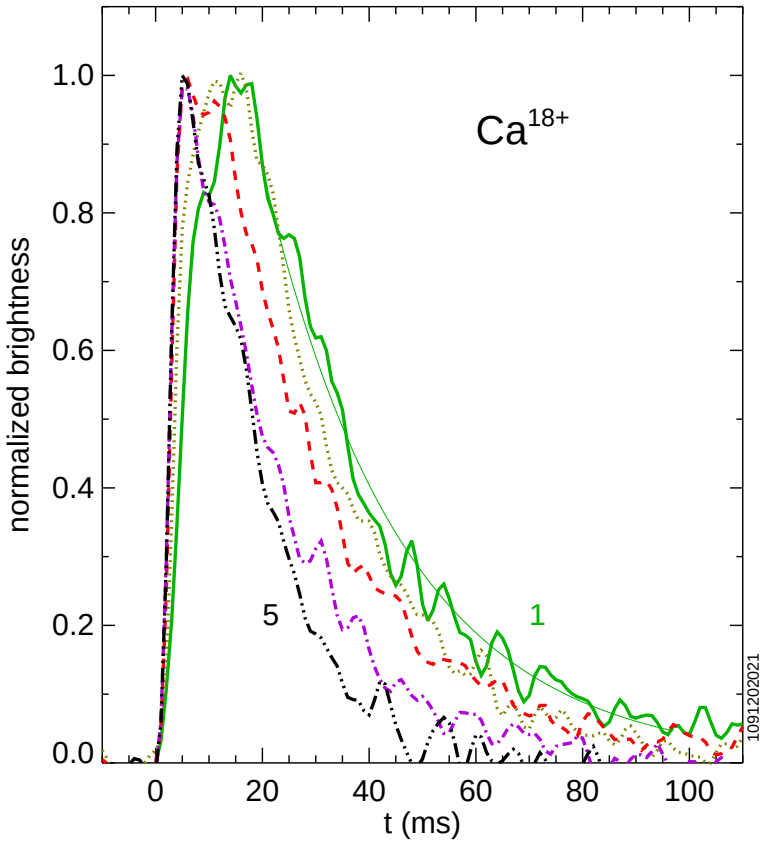


Figure 3: The normalized $Ca^{18+}$ brightness time histories for the five injections from the discharge of Fig.4, shifted such that the injection times (0.565 s, solid green; 0.765 s, mustard dotted; 0.965 s, red dashed; 1.165 s, purple dash-dot; 1.365 s, black chain) are at 0 ms. Shown by the thin green line is an exponential fit to the first injection, with a decay time of 26 ms.

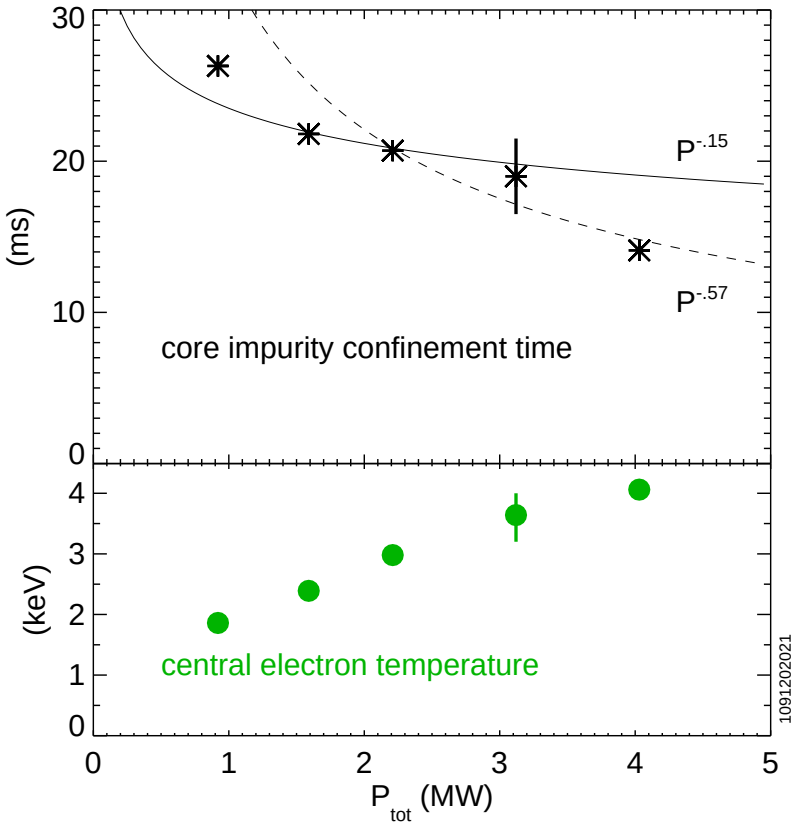


Figure 4: The core impurity confinement time (top) and central electron temperature (bottom) as a function of total Ohmic plus ICRF heating power for the five injections of Fig.2. In the top frame, the solid and dashed curves are proportional to $P_{tot}{}^{-.15}$ and $P_{tot}{}^{-.57}$, respectively, and have been normalized to the point at 2.2 MW.

are systematic increases in the electron (bottom frame) and ion temperatures. Energy confinement is known to degrade with power in ITG mode dominant L-mode plasmas, so this decrease in core impurity confinement may be related.

Whether this anomalous impurity transport is a feature of ITG mode dominated regimes can be investigated by examining impurity confinement across the LOC/SOC boundary. It is widely thought that in the low collisionality LOC regime, TEMs are important in governing transport and that in the high collisionality SOC regime, ITG modes are dominant. The direction of the core rotation velocity has been shown to be a very sensitive indicator of this surprisingly sharp transition [65, 66, 67, 68]. An easy way to cross this boundary is to vary the collisionality by changing the electron density. Shown in Fig.5 are parameter time histories for a 5.4 T, 0.8 MA Ohmic deuterium discharge with $CaF_2$ injections (middle frame) and a density ramp (top frame) which enables the transition from the LOC to the SOC regime (for this current and field the critical transition density is $\sim 0.8 \times 10^{20}/m^3$). In the bottom frame is the central rotation velocity which begins to reverse direction at the critical density (marked by the dotted horizontal line in the top frame). In spite of this change in sign of the core rotation, there is very little effect on the core impurity confinement, as can be seen by comparing the decay phase of the x-ray brightness in the middle frame. There may be some subtle differences in the rise times of the x-ray signals following the injections. It should be noted that these injections were large enough to perturb the electron temperature and density profiles. The results of a systematic shot by shot density scan (at fixed $q_{95}$) across the LOC/SOC boundary are shown in Fig.6. There is very little dependence of the core impurity confinement time on electron density over a range from 0.5 to $1.3 \times 10^{20}/m^3$ for these 5.4 T, 0.8 MA deuterium discharges for which the LOC/SOC boundary is $\sim 0.8 \times 10^{20}/m^3$ [65, 66, 67, 68]. In contrast there is a sign change (reversal) in the core rotation velocity (second frame) and a significant change in slope of the global energy confinement time (top frame). The solid line depicts the neo-Alcator scaling [70], a linear increase with density, and the dashed curve represents the ITER-89 L-mode scaling law [71], very weakly dependent on density (saturated). This is the origin of the names LOC and SOC. There is also a noticeable change in the electron density scale length at the mid radius (third frame); the profiles become increasingly peaked in the LOC regime, then saturate and flatten after the transition [66, 72, 67, 68]. The relative insensitivity to density in the bottom frame suggests that core impurity confinement has a similar behavior in both TEM and ITG mode dominant Ohmic L-mode regimes [46].

The mustard asterisks in the bottom frame of Fig.6 are the impurity confinement times from hydrogen plasmas; there is very little difference between the impurity confinement times in hydrogen and deuterium Ohmic L-mode plasmas. Shown in Fig.7 is the impurity confinement time as a function of the average mass of the working gas for 5.4 T, 0.8 MA Ohmic L-mode plasmas. The electron densities were in the range from $0.5\text{-}0.6 \times 10^{20}/m^3$. The working gas mass was determined from the measured brightness ratios of H to D Balmer $\alpha$. There is typically about a 10% hydrogen fraction in nominal deuterium plasmas. This independence of impurity confinement time on background ion mass in these L-mode plasmas is in contrast to the trends previously observed in circular, limited discharges [28, 29].

The core impurity confinement time in Ohmic plasmas has been found to increase

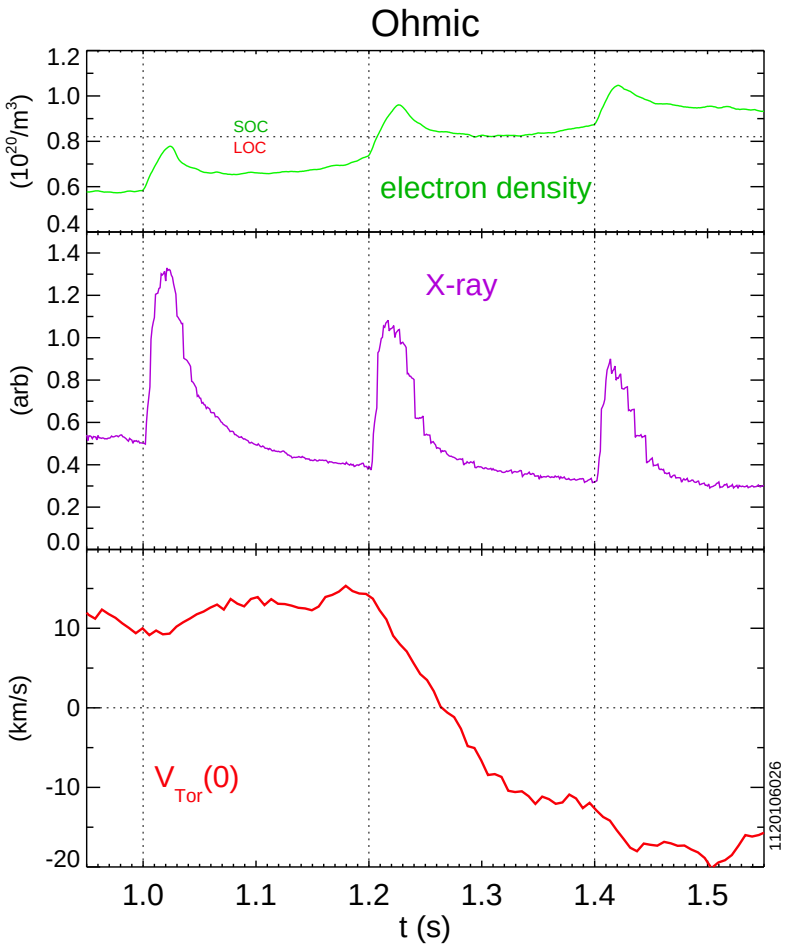


Figure 5: Time histories of the electron density (top), soft x-ray brightness (middle) and core rotation velocity (bottom) for a 5.4 T, 0.8 MA deuterium discharge with $CaF_2$ injections at 1.0, 1.2 and 1.4 s.

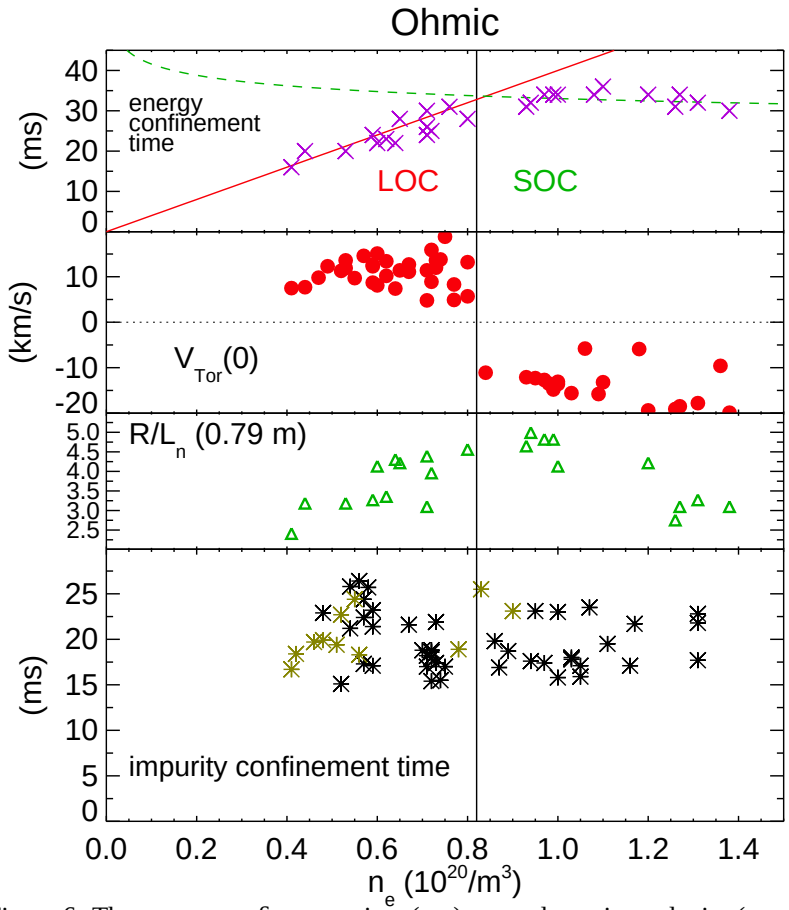


Figure 6: The energy confinement time (top), central rotation velocity (second frame), normalized inverse electron density scale length at the mid radius (third frame) and core impurity confinement time (bottom) as a function of electron density for 5.4 T, 0.8 MA deuterium discharges (black asterisks). The solid line in the top frame depicts the neo-Alcator scaling and the dashed curve represents the ITER-89 L-mode scaling law. The vertical line at $n_e$=0.82$\times 10^{20}$/m$^3$ indicates the critical density for rotation reversal, which also marks the transition between the LOC and SOC regimes where the two scaling laws cross. Shown by the mustard asterisks in the bottom frame are the impurity confinement times for hydrogen plasmas.

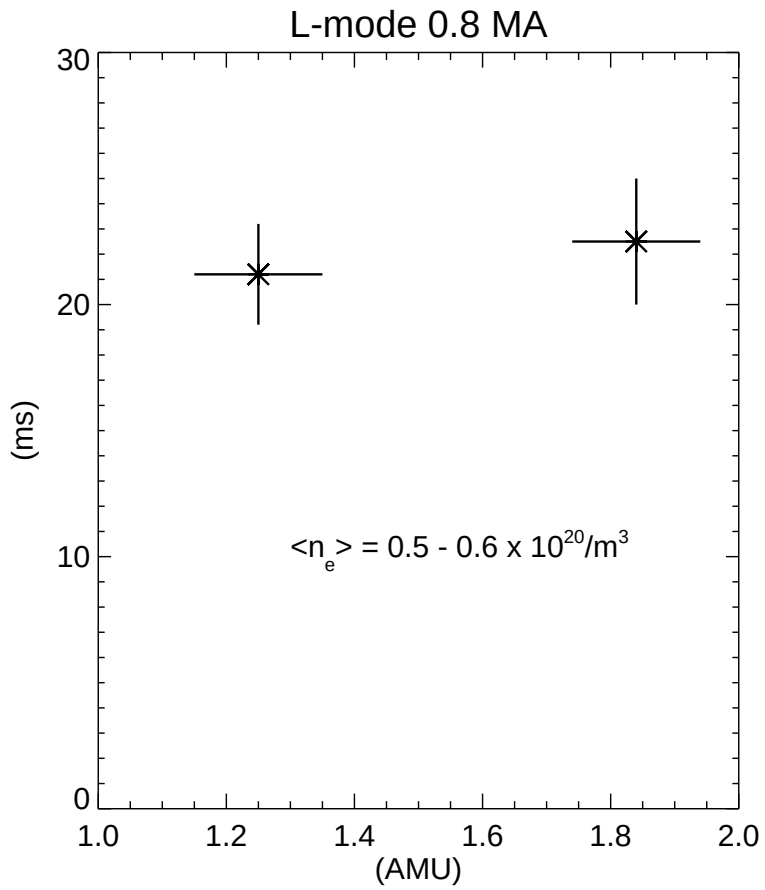


Figure 7: The core impurity confinement as a function of background ion mass for 5.4 T, 0.8 MA Ohmic L-mode plasmas.

with increasing plasma current at fixed magnetic field [28, 29, 35, 73]. Similar behavior is exhibited in ICRF heated L-mode discharges [43], as seen in Fig.8, which is a comparison of 5.4 T deuterium plasmas with 1.0 MW of ICRF power at currents 0.6 and 1.0 MA, each with five $CaF_2$ injections. It can be clearly seen that the higher

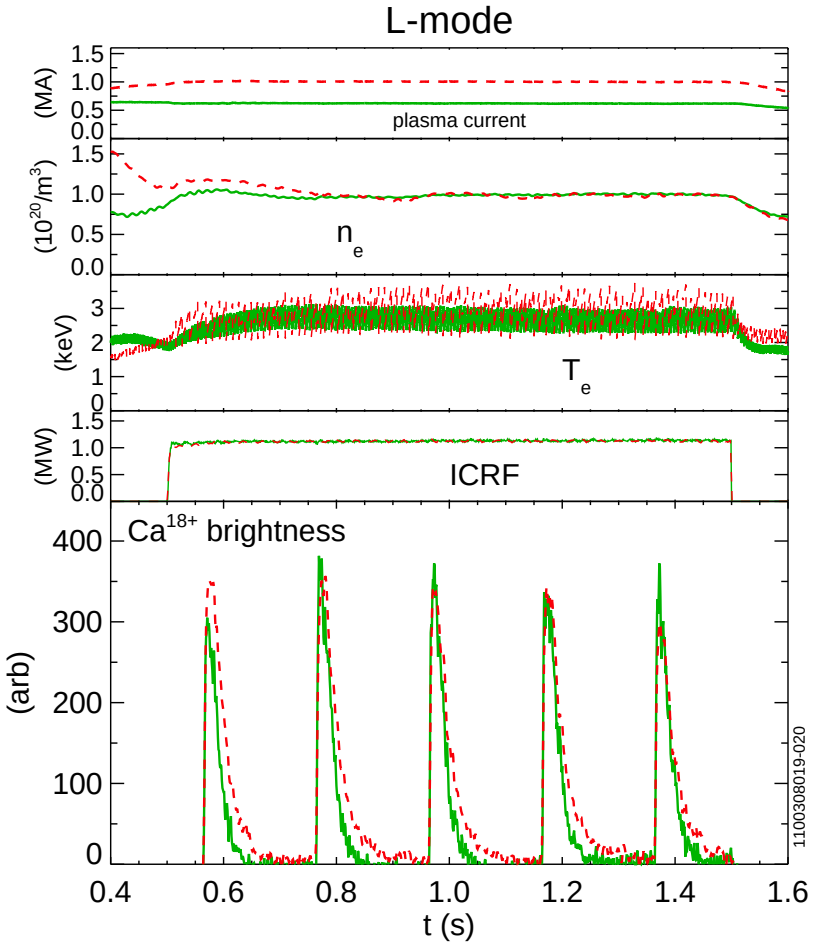


Figure 8: Time histories of the plasma current, electron density, central electron temperature, ICRF power and $Ca^{18+}$ brightness for 5.4 T deuterium discharges at 0.6 MA (solid green) and 1.0 MA (red dashed).

plasma current discharge has longer impurity confinement times. The results of the complete plasma current scan for 5.4 T deuterium discharges with $<n_e>$ = $1\times10^{20}/m^3$ and 1.0 MW of ICRF power are shown in Fig.9, capturing the same trend as seen in purely Ohmic plasmas. The solid curve is proportional to $I_p{}^{.68}$ which was found from a regression analysis of C-Mod data [43]; the dashed curve is proportional to $I_p{}^{.31}$ which was derived from observations from JET and Tore Supra [35]. This dependence on plasma current has been reproduced in gyro-kinetic simulations of impurity

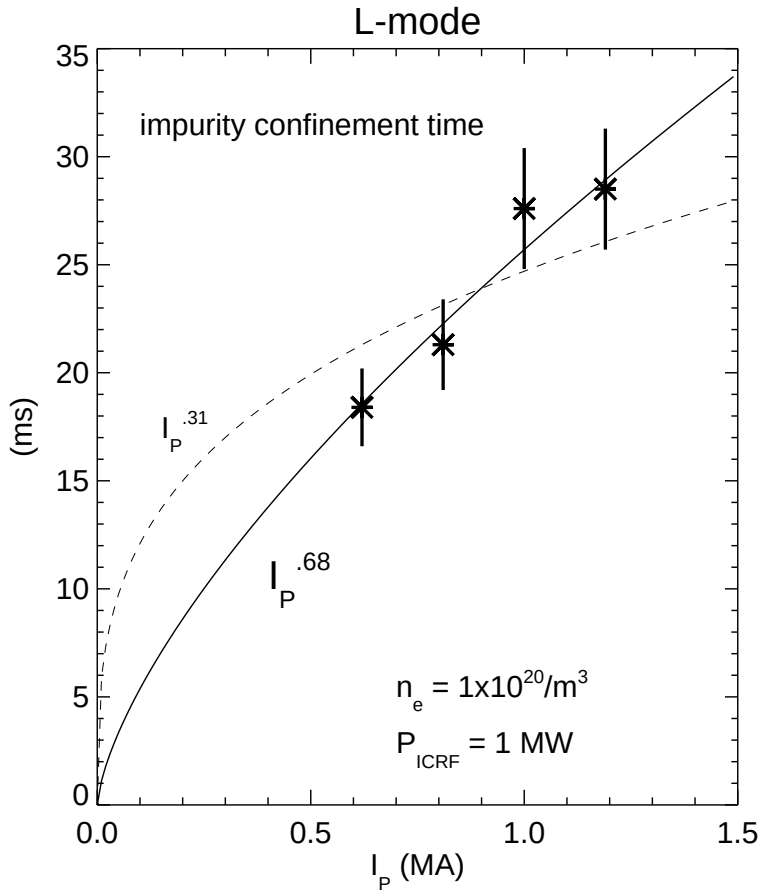


Figure 9: The core impurity confinement time as a function of plasma current for 5.4 T deuterium L-mode discharges with 1.0 MW of ICRF power at an electron density of $1.0\pm0.1\times10^{20}/\mathrm{m}^3$. The solid curve is proportional to $\mathrm{I_p}^{.68}$ and the dashed curve represents $\mathrm{I_p}^{.31}$.

confinement in the core temperature gradient region ($0.3 < r/a < 0.6$) [43] in C-Mod discharges. Whether it is a coincidence that this similar trend holds in the plasma center where the gradients are weak is not known.

The dependence of the core impurity confinement time on toroidal magnetic field has also been investigated. Shown in Fig.10 is a comparison of parameter time histories for two 0.8 MA deuterium Ohmic discharges ($<n_e> = 1.0\times10^{20}/m^3$) with magnetic fields of 3.3 and 6.5 T. There is very little difference in the $Ca^{18+}$ brightness time

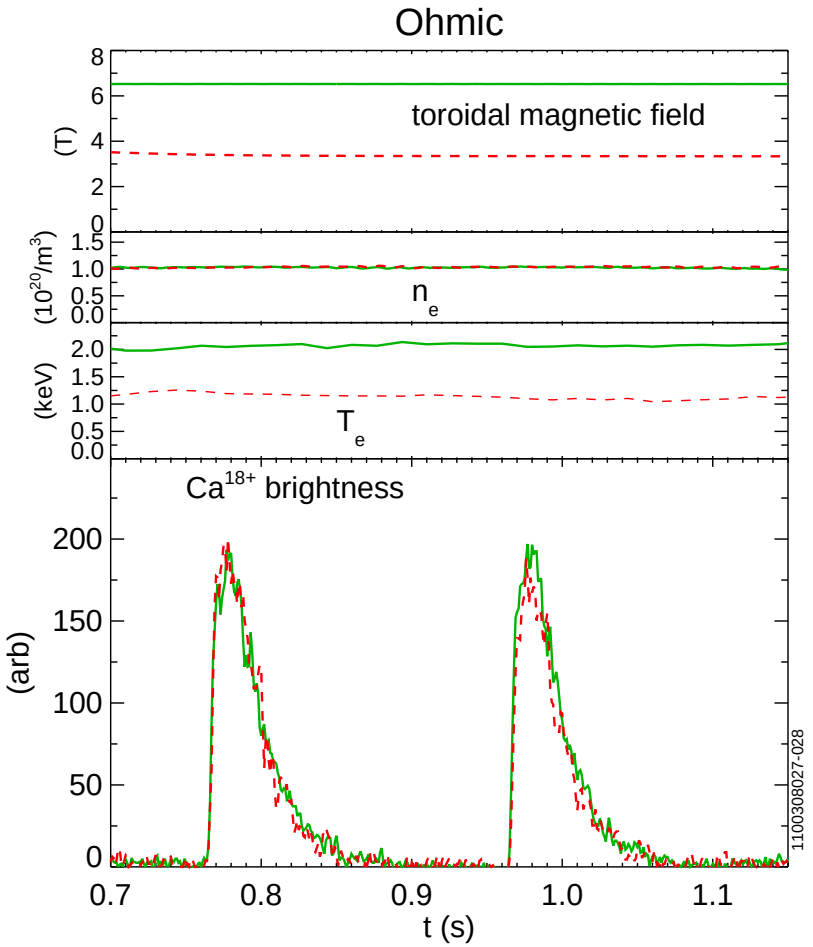


Figure 10: Time histories of the toroidal magnetic field, electron density, central electron temperature and $Ca^{18+}$ brightness for 0.8 MA deuterium Ohmic discharges at 6.5 (solid green) and 3.3 T (red dashed).

histories and impurity confinement times with a factor of two change in the toroidal magnetic field. The results of the full magnetic field scan are shown in Fig.11, along with a curve proportional to $B_T{}^{.18}$, a scaling which was derived from a regression analysis of C-Mod data [43]. This scaling is in contrast to the observations from Alcator C

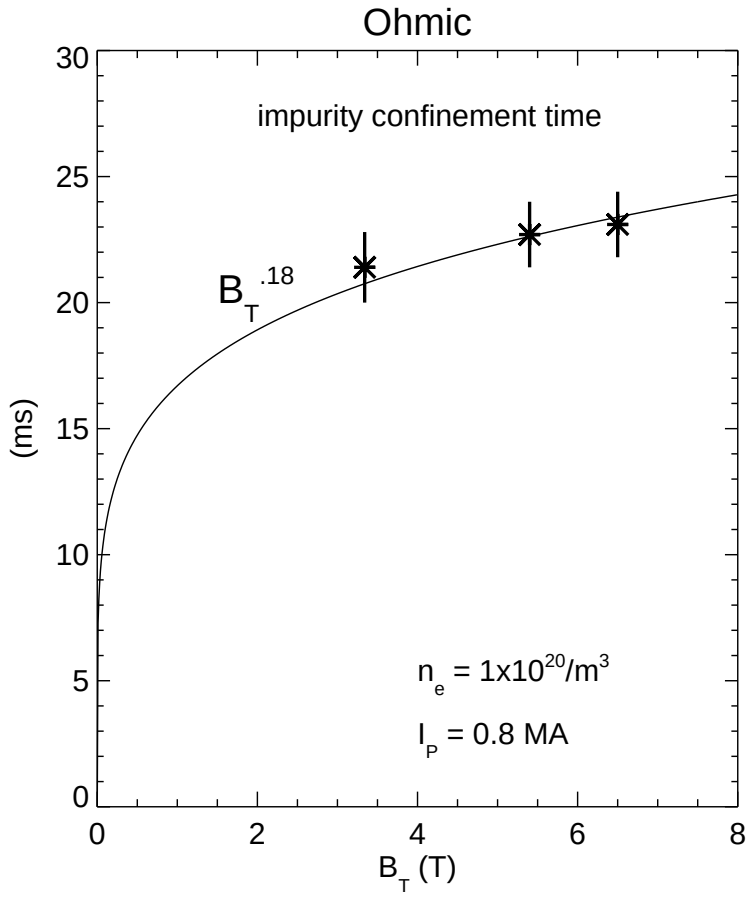


Figure 11: The core impurity confinement time as a function of toroidal magnetic field for 0.8 MA deuterium discharges at an electron density of $1.0\times10^{20}$/m$^3$. The solid curve is proportional to $B_T{}^{0.18}$.

[29] and TCV [38] which showed a marked drop in the impurity confinement time as the toroidal magnetic field was increased. The relatively strong plasma current dependence of impurity confinement and weak dependence on magnetic field suggest that the inverse rotational transform q is not the governing parameter.

The influence of sawteeth on core impurity confinement has been investigated with the use of external magnetic field perturbation coils [56], which can induce locked modes that lead to a suppression of sawteeth and a braking of the core toroidal rotation [74]. Shown in Fig.12 is a comparison of parameter time histories for two 5.4 T 0.8 MA deuterium Ohmic L-mode target plasmas at $<n_e> = 0.9\times10^{20}/m^3$, one with A coils applied to suppress sawtooth oscillations. The overall impurity behavior, including core

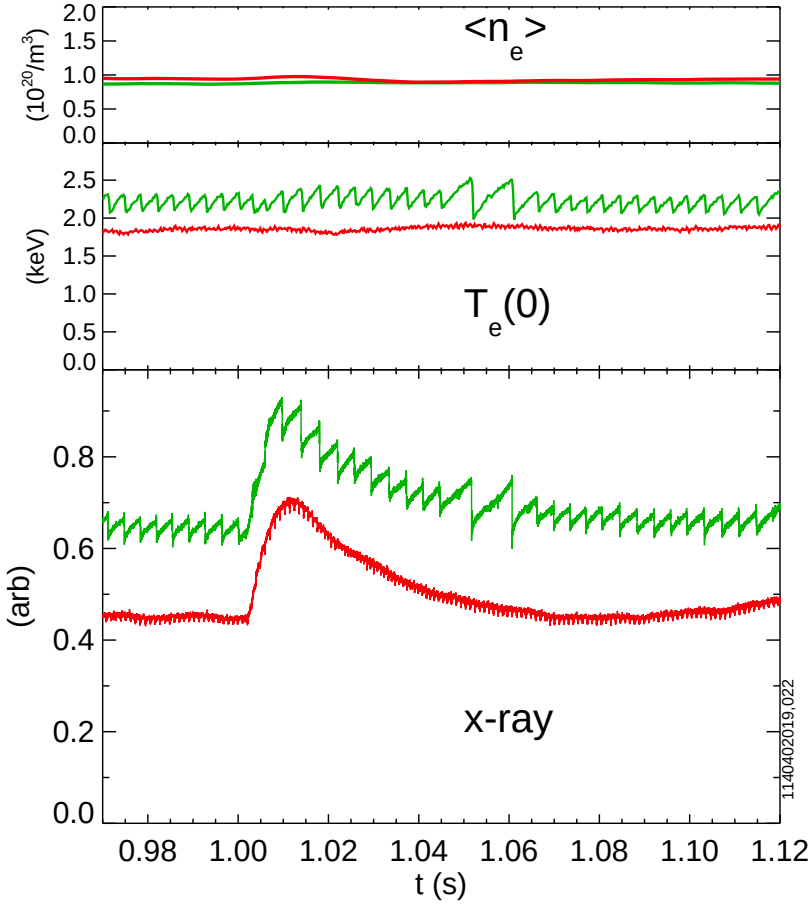


Figure 12: From top to bottom, time histories of the average electron density, central electron temperature and central chord x-ray brightness for two 5.4 T, 0.8 MA deuterium Ohmic discharges with (red) and without (green) external field coil application. $CaF_2$ injections were at 1.0 s.

impurity confinement time, is quite similar in both cases despite the suppression of sawteeth. This indicates that in this particular case of a locked mode plasma, sawteeth do not have much of an effect on core impurity transport, in contrast to earlier studies [75]. However, to study in detail the effects of sawteeth on core impurity confinement, time resolved impurity profile measurements are necessary on a time scale short compared to the sawtooth period. A comparison of discharges with sawtooth stabilization from lower hybdrid current drive would also be informative.

The bottom line from this section is that impurity confinement times are relatively short in L-mode plasmas, and impurity accumulation is not a problem.

## IV. I-mode

I-mode is an enhanced confinement regime which features the energy confinement of H-mode with the particle and impurity confinement properties of L-mode [47, 48, 49, 50, 51, 52]. This is manifested in the presence of a steep edge temperature gradient without a steep edge density gradient, a separation of the energy and particle transport channels which are coupled in H-mode. The prescription to attain I-mode with auxiliary heating is simply to operate in the 'unfavorable' configuration, with the active X-point opposite to the ion $B\times\nabla B$ drift direction. The plasma of Fig.2 actually entered I-mode with the last two steps of ICRF heating power, identified by the formation of an edge temperature pedestal with a gradient in excess of $\sim$40 keV/m and the appearance of an edge weakly coherent mode with frequency $\sim$100-200 kHz. There is no clear signature of the L-I transition such as an abrupt change in edge $D_\alpha$ light, which is often observed at the transition to H-mode.

Injections into a steady I-mode plasma (1.1 MA, 5.5 T, $q_{95}$ = 3.2) are presented in Fig.13. There was a substantial increase in the stored energy (top frame) due to an increase in the core electron temperature and the formation of an edge temperature pedestal, with a gradient of $\sim$140 keV/m. There was no change in the electron density ($<n_e>$ = $1.2\times10^{20}/m^3$) and no density pedestal formation (gradient $<10^{22}/m^4$). The average of core impurity confinement times for the four injections was 26.5 ms, similar to typical L-mode values. In this case the core impurity confinement time was determined from H-like $Ca^{19+}$ since at these high electron temperatures He-like $Ca^{18+}$ was burned out in the plasma center. A major advantage of I-mode is the L-mode impurity confinement exhibited simultaneously with H-mode energy confinement. $H_{98}$ [76] for this discharge was 1.0. In addition to the similar magnitude of impurity confinement time, scalings with plasma parameters in I-mode are reminiscent of those seen in L-mode. Shown in Fig.14 is the core impurity confinement time as a function of plasma current for deuterium I-mode discharges at 5.4 T and fixed electron density. Unfortunately there are very few I-mode discharges at low plasma current. However, there is a definite increase in the impurity confinement time with increasing plasma current, as was observed in L-mode.

Injection of molybdenum into I-mode plasmas reveals information about the transport dependence on impurity mass and/or charge. Shown in Fig.15 is the core impurity confinement time as a function of atomic mass for 1.0 MA deuterium I-mode plasmas

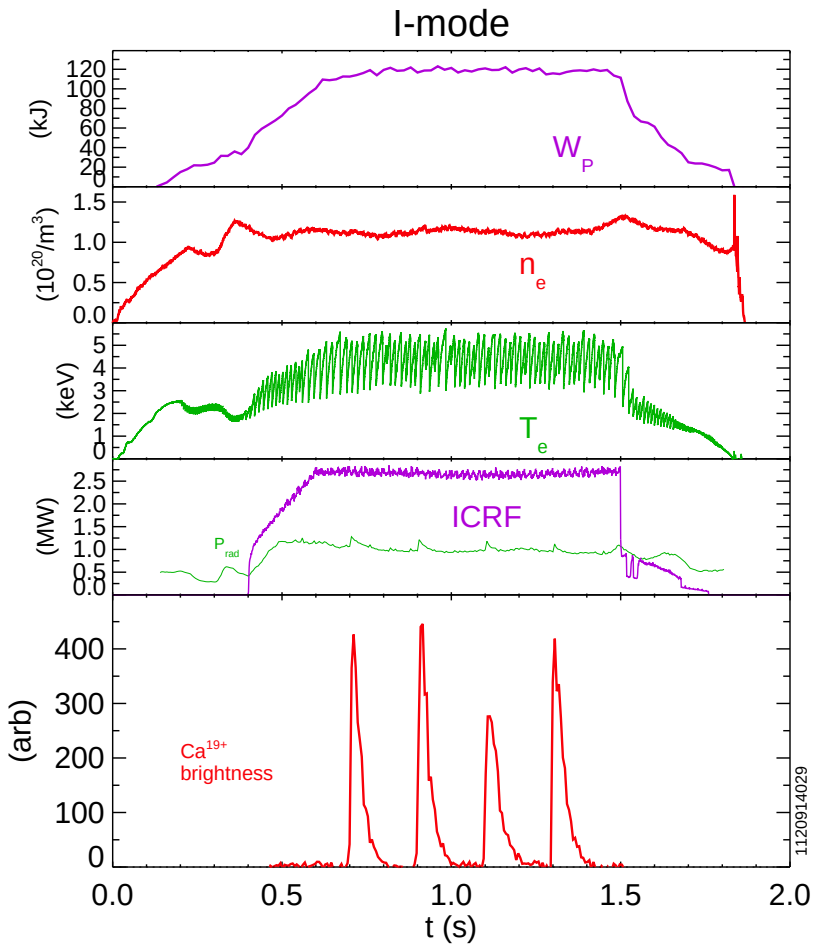


Figure 13: Parameter time histories for a 5.5 T, 1.1 MA deuterium I-mode discharge with four $CaF_2$ injections. From top to bottom, the plasma stored energy, average electron density, central electron temperature, ICRF power (and radiated power) and $Ca^{19+}$ brightness. Injection times were 0.7, 0.9, 1.1 and 1.3 s.

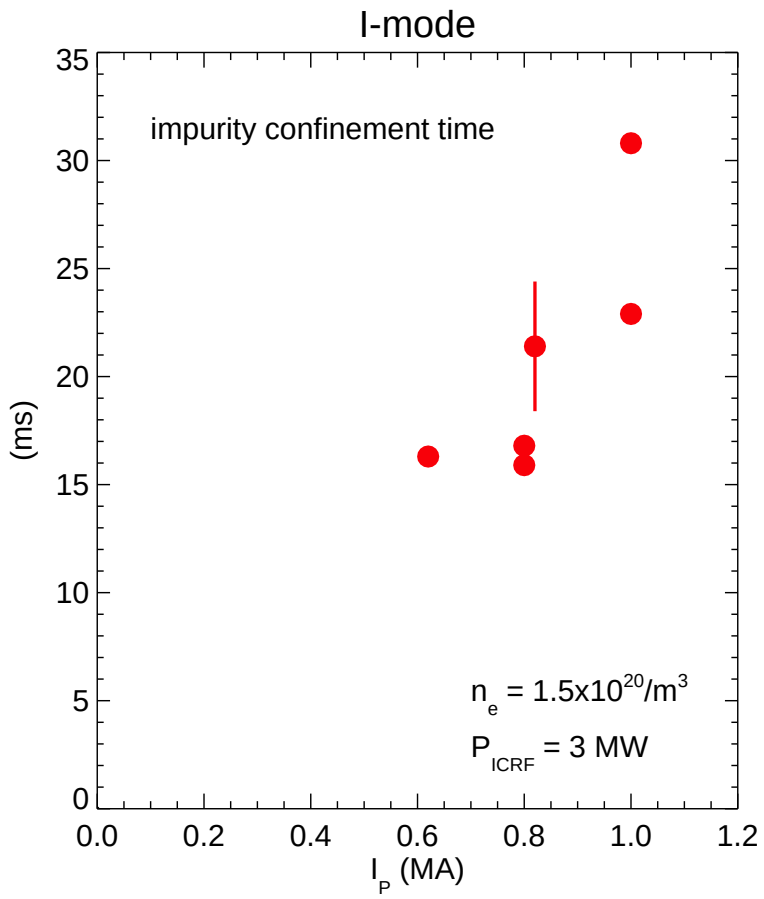


Figure 14: The core impurity confinement time as a function of plasma current for 5.4 T deuterium I-mode plasmas with $<n_e> = 1.5\times10^{20}/m^3$.

with magnetic fields between 5.4 and 5.8 T and $<n_e>$ = $1.5\pm0.2\times10^{20}/m^3$. There

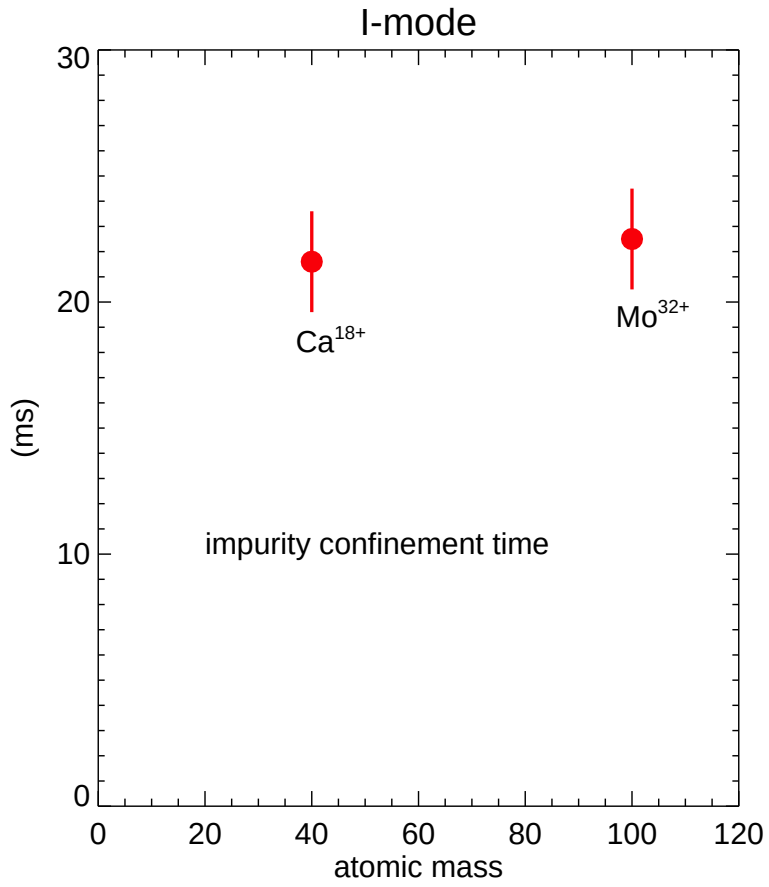


Figure 15: The core impurity confinement time as a function of atomic mass for 1.0 MA I-mode plasmas with $B_T$ between 5.4 and 5.8 T and $<n_e>$ between 1.3 and $1.7\times10^{20}/m^3$.

is very little dependence on impurity mass, which is similar to observations in Ohmic L-mode discharges [29, 35]. These measurements were from helium-like calcium and neon-like molybdenum, so the charge to mass ratio only varied from 0.45 to 0.32, not a large range in this quantity. Overall, impurity confinement in I-mode is very similar to that found in L-mode, and impurity accumulation is not an issue.

**V. H-mode**

H-mode has been chosen as the operational regime for ITER [77] because of its good energy confinement properties. Unfortunately, impurity confinement times are much longer in H-mode plasmas, as mentioned in the introduction. For Alcator C-Mod, a particular variety of H-mode (EDA H-mode [78]) has been studied extensively. An example of the core impurity transport properties is demonstrated in Fig.16 showing a single $CaF_2$ injection into a 5.4 T, 0.8 MA deuterium EDA H-mode discharge. In this

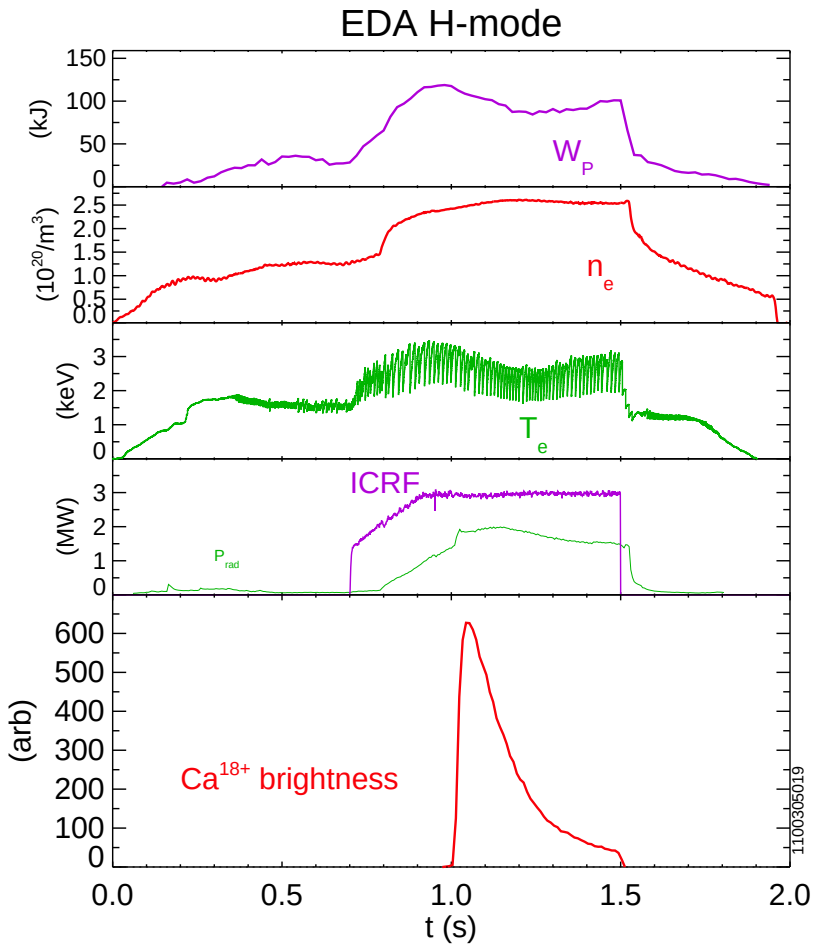


Figure 16: Parameter time histories for a 5.4 T, 0.8 MA deuterium EDA H-mode discharge with a single $CaF_2$ injection (1.0 s). From top to bottom, the plasma stored energy, average electron density, central electron temperature, ICRF power (and radiated power) and $Ca^{18+}$ brightness.

case the core impurity confinement time was 154 ms, nearly an order of magnitude longer than seen in the I-mode plasma of Fig.13, which had the same ICRF power and Ohmic target density, similar stored energy and $H_{98}$ confinement factor. In EDA H-mode there are increases in both the electron density and temperature which contribute

to the increased stored energy, and the formation of edge pedestals in both density and temperature. This longer impurity confinement time is due partially to reduced core diffusivity but mainly due to the presence of a neo-classical-like inward pinch in the vicinity of the pedestal density gradient [8, 9, 11, 12, 13, 15, 16, 18, 19]. In L- and I-mode plasmas, there is no density pedestal [47, 48, 49, 79, 80] and hence no strong inward impurity pinch at the edge.

Although the magnitude of the core impurity confinement time is much longer in H-mode, the scaling with plasma current appears to be similar to that observed in L- and I-mode plasmas. This is demonstrated in Fig.17, which is a comparison of the normalized $Ca^{18+}$ brightness time histories from three 5.4 T deuterium EDA H-mode discharges with different plasma currents. There is a strong reduction in impurity confinement

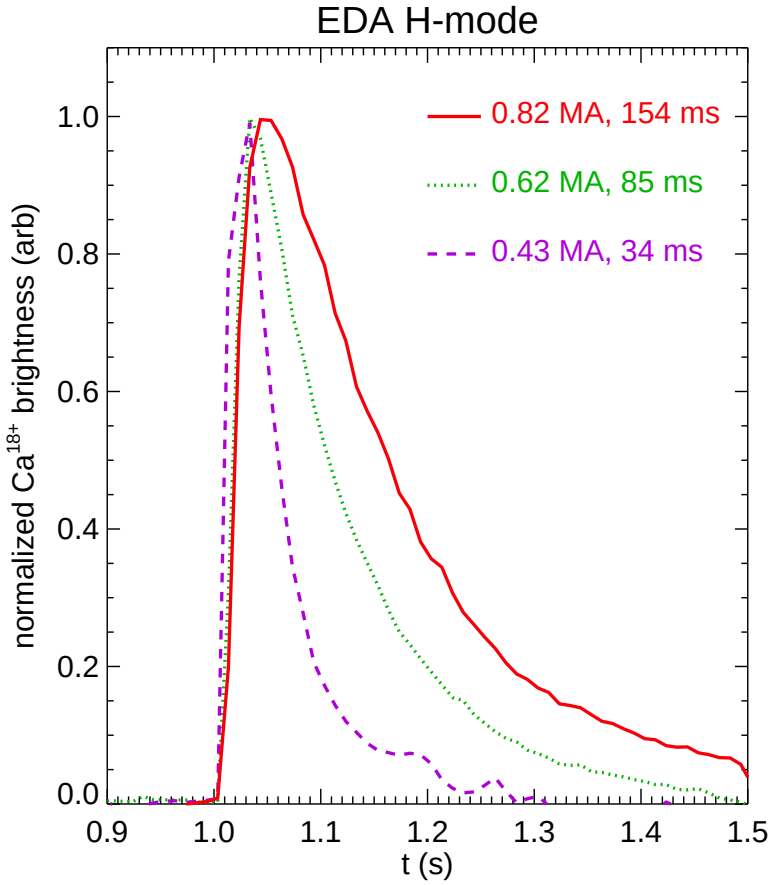


Figure 17: Normalized $Ca^{18+}$ brightness time histories from three 5.4 T deuterium EDA H-mode discharges with plasma currents of 0.82 (solid red), 0.62 (dotted green) and 0.43 MA (dashed purple).

time as the plasma current is lowered. This is not an entirely clean comparison, since due to a lack of density control in H-mode plasmas, these three discharges had three different electron densities: $2.5\times10^{20}/m^3$ for 0.82 MA, $1.8\times10^{20}/m^3$ for 0.62 MA and $1.4\times10^{20}/m^3$ for 0.43 MA. It is not possible to rule out a potential density dependence of the impurity confinement time in H-mode plasmas. The scaling of the core impurity confinement time with plasma current for a series of 5.4 T deuterium EDA H-mode discharges is shown in Fig.18. There is an apparent strong dependence of impurity

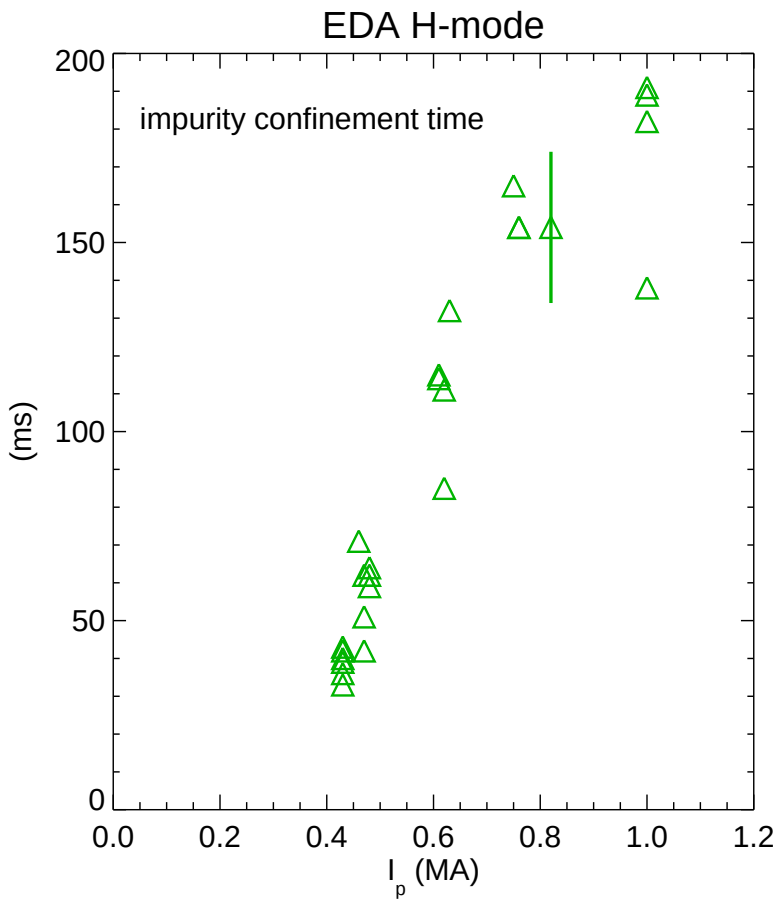


Figure 18: The core impurity confinement time as a function of plasma current for 5.4 T deuterium EDA H-mode discharges, unsorted for electron density.

confinement time with plasma current in EDA H-mode discharges, similar to what is observed in L- and I-mode, although for the H-mode discharges, the electron density was not held constant during the current scan.

Information regarding the impurity confinement dependence on impurity mass has been addressed by injecting tungsten into EDA H-mode plasmas [62]. The subsequent

tungsten emission has been monitored with the soft x-ray array, which is sensitive to 3d - 4f transitions near 6 Å in charge states between $W^{40+}$ and $W^{48+}$ [81] for core electron temperatures between 1.5 and 3.5 keV. The core impurity confinement time as a function of injected impurity mass is shown in Fig.19 for 5.4 T, 0.6 MA deuterium EDA H-mode discharges with $<n_e>$ between 1.8 and $2.3\times10^{20}/m^3$. There does not

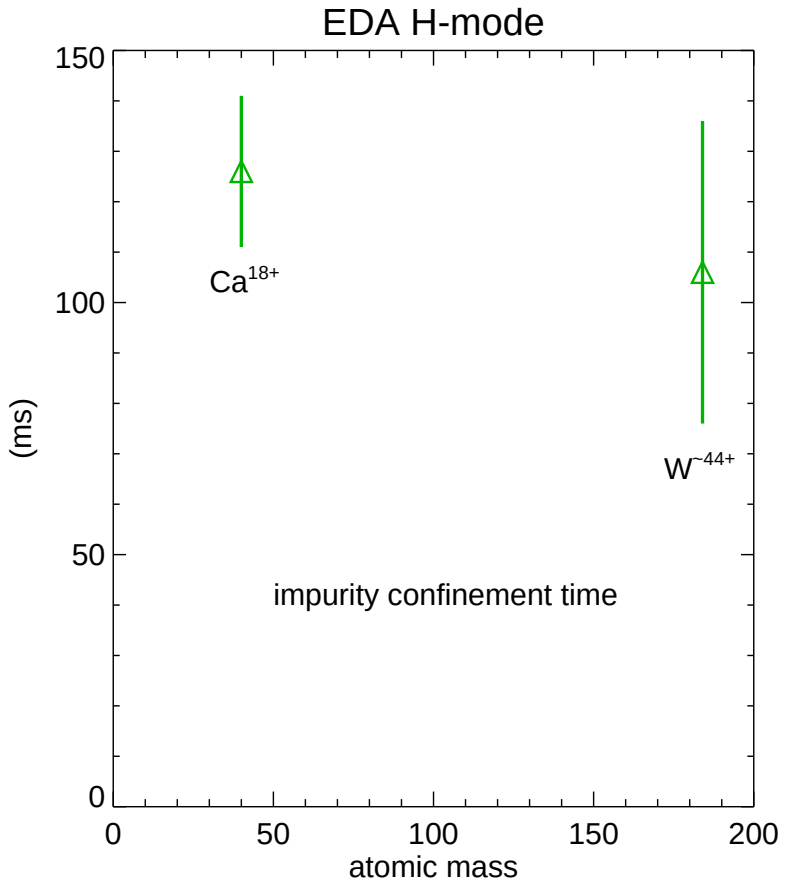


Figure 19: The core impurity confinement time as a function of injected impurity mass for 5.4 T, 0.6 MA deuterium EDA H-mode discharges, with electron density between 1.8 and $2.3\times10^{20}/m^3$.

seem to be much dependence of core impurity confinement on impurity mass.

One defining feature of EDA H-mode is the presence of the Quasi-Coherent Mode, an electron drift wave residing near the last closed flux surface [82], which is thought to regulate particle transport in the absence of ELMs. There are no such pedestal relaxation mechanisms in ELM-free H-modes, and as such these plasmas are transient in nature, suffering from impurity build-up and radiative collapse. An example of ex-

tremely long impurity confinement in an ELM-free H-mode [11, 57] (5.5 T, 0.9 MA deuterium) is shown in Fig.20. Following the $CaF_2$ injection at 1.2 s, the plasma (re-

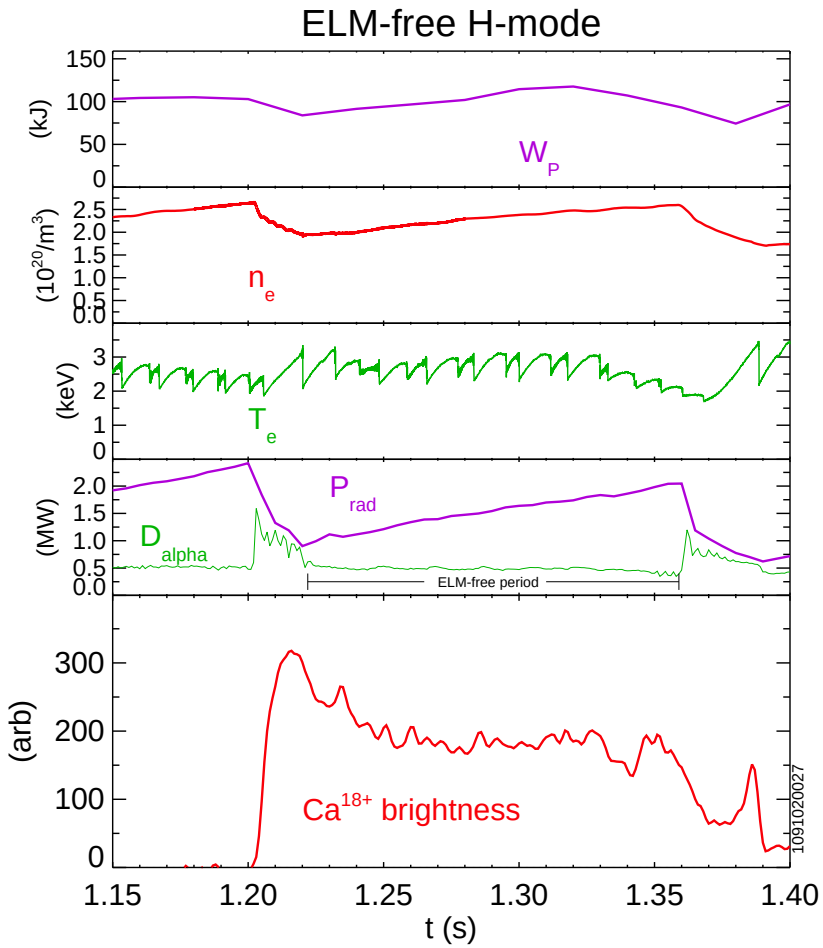


Figure 20: Parameter time histories for a 5.5 T, 0.92 MA deuterium ELM-free (between 1.22 and 1.36 s) H-mode discharge with a single $CaF_2$ injection (1.2 s). From top to bottom, the plasma stored energy, average electron density, central electron temperature, radiated power (and $D_\alpha$ brightness) and $Ca^{18+}$ brightness.

)entered ELM-free H-mode at 1.22 s (see $D_\alpha$ brightness). Unlike the Ohmic, L-, I- and EDA H-mode cases, the $Ca^{18+}$ brightness did not decay, but remained constant, indicating impurity accumulation [11] (and an ill defined and very long impurity confinement time, $\sim$700 ms from a fit). During the time interval from 1.22 to 1.36 s, there was a steady increase in the electron density and a factor of two increase in the radiated power (a substantial fraction of the 3 MW from ICRF), which led to the collapse of the H-mode. The long impurity confinement in H-mode, with the potentially dangerous neo-classical pinch for high Z materials, should raise red flags.

## VI. Discussion

In an effort to unify observations across the different confinement modes, various metrics have been compared. For example, particle (impurity) confinement is sometimes connected to energy confinement. The core impurity confinement time (from calcium injections) as a function of confinement factor $H_{89}$ is shown in Fig.21. For

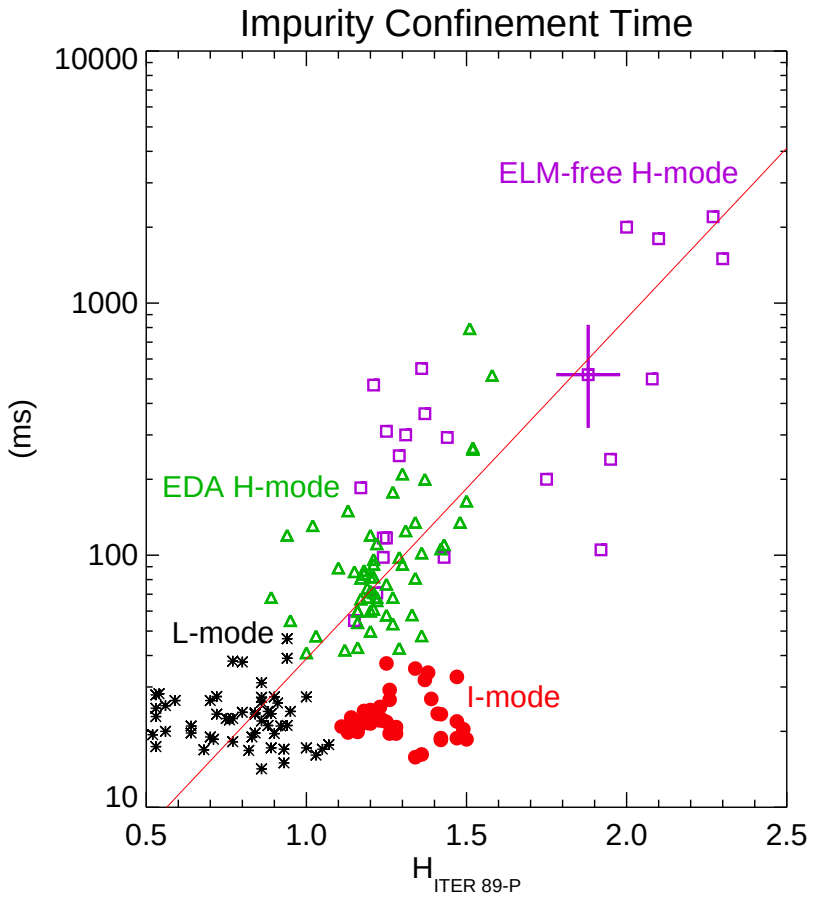


Figure 21: A log plot of the core impurity confinement time as a function of energy confinement factor $H_{89}$ for L-mode (asterisks), I-mode (dots), EDA H-mode (triangles) and ELM-free H-mode (squares). The line is a fit to the L- and H-mode points.

L- and H-mode, there is a very strong correlation between impurity and energy confinement [19], as shown by the solid line. This connection is broken in I-mode, which combines the good energy confinement of H-mode with the poor (but favorable) impurity confinement of L-mode; this is one of many attributes of I-mode which makes it superior to H-mode. For comparison, the core impurity confinement time as a function

of confinement factor $H_{98}$ is shown in Fig.22. These points represent the full range of

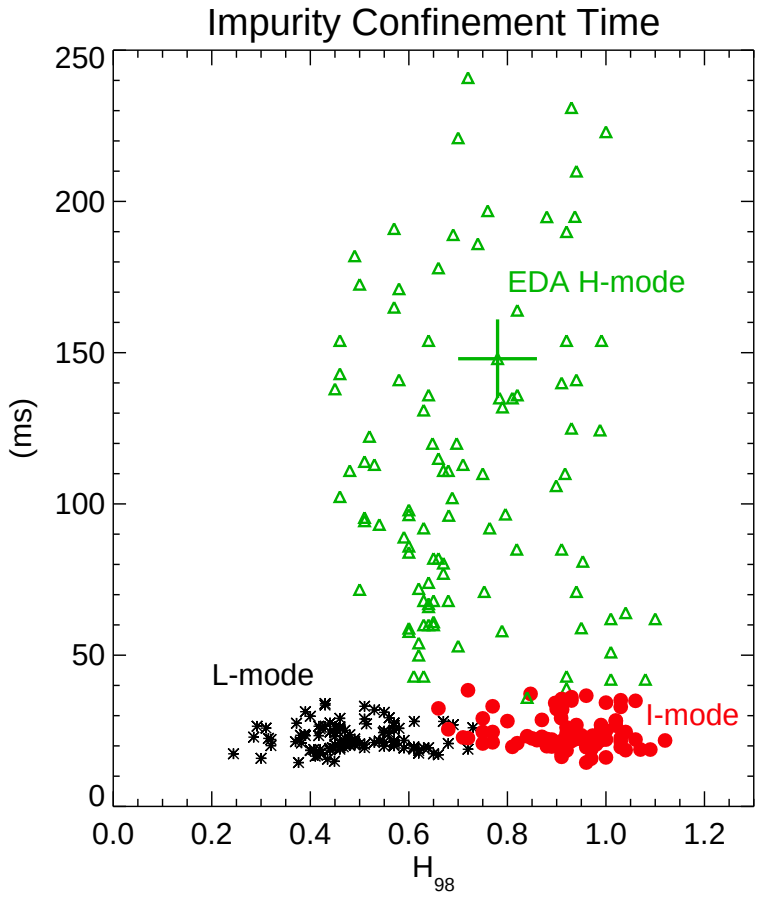


Figure 22: The core impurity confinement time as a function of energy confinement factor $H_{98}$ for L-mode (asterisks), I-mode (dots) and EDA H-mode (triangles).

plasma current, toroidal magnetic field, electron density and ICRF power. There is a bit of overlap between the L- and I-mode points; there is no sharp power threshold for entering I-mode as there is for H-mode. The I-mode points exhibit impressive values of $H_{98}$ with the excellent impurity confinement properties of L-mode. It should be noted that many C-Mod H-mode discharges do not follow the $H_{98}$ scaling law [76] (or $H_{89}$), which contributes to the large range of H factors.

One fundamental difference between I- and H-mode is that there is no density pedestal in I-mode. Impurity confinement time scaling with edge density gradient does a better job of unifying L-, I- and H-mode observations, as shown in Fig.23. There is a strong correlation between the two quantities and in constrast to Figs.21 and 22, the L- and I-mode points overlap. This dependence of impurity confinement time on

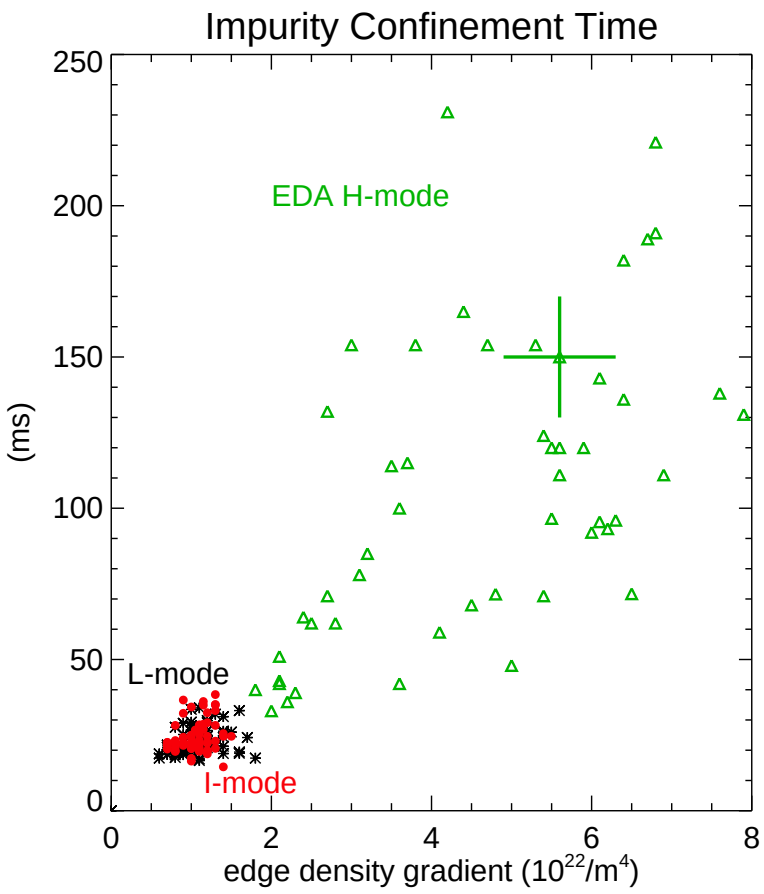


Figure 23: The core impurity confinement time as a function of edge density gradient for L- (asterisks), I- (dots) and H-mode (triangles) plasmas.

edge density gradient actually explains the apparent scaling with plasma current in EDA H-mode plasmas (Fig.18). There is a strong connection between pedestal density gradient and plasma current in EDA H-mode plasmas [83], as demonstrated in Fig.24. The large density gradients at the edge of H-mode plasmas give rise to a substantial

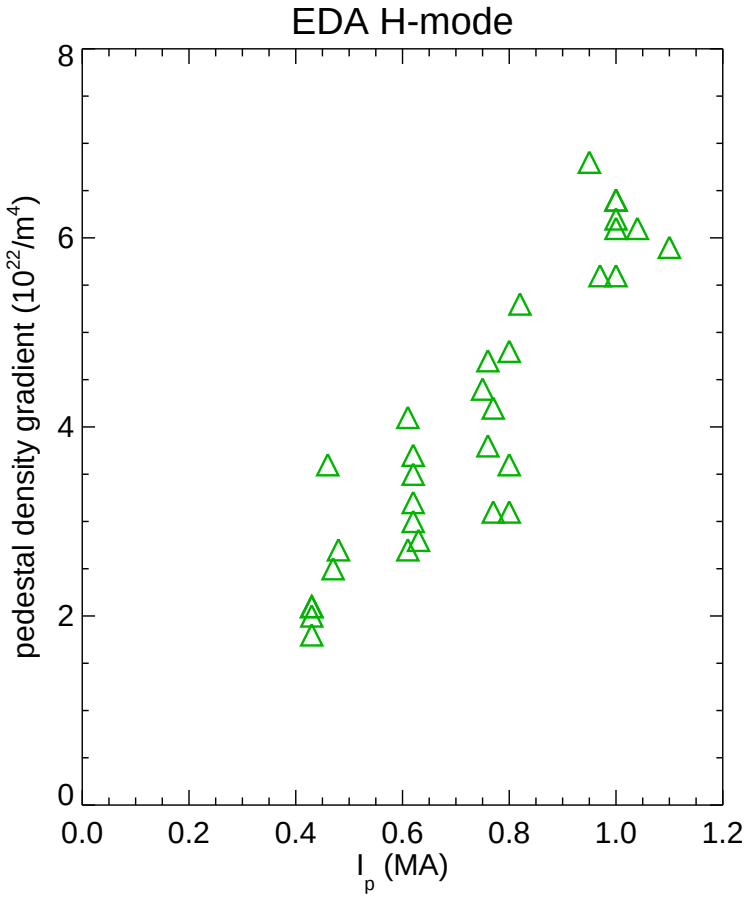


Figure 24: The pedestal density gradient for EDA H-mode plasmas as a function of plasma current, for discharges with impurity injection.

inward neo-classical impurity pinch, which leads to long impurity confinement times. This implies that the large inward impurity convection at the edge dominates the core impurity confinement times [75]. Similar behavior is seen in the core of plasmas with ITBs.

A summary of the impurity confinement results for different operational regimes is presented in Table 1. In the second column is the range of $D_{eff}$ derived from the core impurity confinement time shown in the first column. This may not be strictly applicable for the H-mode discharges where the confinement times are dominated by

| regime | $\tau_I$ (ms) | $D_{\rm eff}$ ($m^2$/s) | max V (m/s) | [Refs.] | strong dep. | weak dep. | drive |
|---|---|---|---|---|---|---|---|
| Ohmic L- LOC | 15-27 | 0.28-0.50 | | | | $n_e$ | TEM? |
| Ohmic L- SOC | 15-27 | 0.28-0.50 | $\sim$0 | [11] | $I_p$ | $n_e$ | ITG |
| ICRF L- | 15-35 | 0.22-0.50 | | | $I_p$ | $B_T$ | ITG |
| ICRF I- | 15-35 | 0.22-0.50 | | | $I_p$ | $M_Z$ | ITG |
| EDA H- | 35-300 | 0.025-0.22 | -10 | [11] | $\nabla$n | $M_Z$ | neo-cl |
| ELM-free H- | 50-3000 | 0.0025-0.15 | -30 | [11] | | | neo-cl |
| ITB | accum. | | -100 | [14] | | | neo-cl |

Table 1: Impurity confinement properties for different C-Mod operational regimes.

the edge impurity pinch. In the $3^{\rm rd}$ column are previously derived values for the inward convection, with C-Mod references given in the $4^{\rm th}$ column. The $5^{\rm th}$ and $6^{\rm th}$ columns indicate the strongest and weakest scalings with plasma parameters, respectively. In the last column is listed the predominant drive for transport. For most L- and I-mode plasmas, ITG modes dominate. In regimes with turbulence suppression and transport barrier formation, neo-classical effects dominate in the barrier regions; in the edge for H-mode and near the mid radius for ITB plasmas.

Turbulence drives which rely on temperature and density gradients are small in the very core (r/a $<$ 0.3) but may be significant in the steeper gradient regions (0.3 $<$ r/a $<$ 0.6) [43]. The quantity $\eta \equiv L_n/L_T$ = n$\nabla$T/T$\nabla$n is a measure of the relative impact of the temperature and density gradients. The radial profile of $\eta$ for electrons is shown by the solid curve in Fig.25 for typical Ohmic L-mode density and temperature profiles. In the mid radius region of this Ohmic L-mode discharge, $\eta$ varies between 1 and 3.5; inside of r/a = 0.2 both the temperature and density profiles are very flat, and it is difficult to evaluate $\eta$. Profiles of $\eta$ for ions are similar insofar as the electron and ion temperature profiles are similar; ion density profiles are not measured in C-Mod. The radial profile of $\eta$ for electrons for a typical I-mode plasma is also shown by the red dotted line, and ranges between 1.5 and 3.5. For a typical H-mode discharge, the $\eta$ profile for electrons is shown for comparison by the dashed green line, and ranges from 2.5 to 5.

## VII. Conclusions

The core impurity confinement properties of L-, I- and EDA H-mode plasmas have been investigated using laser blow-off of Ca, Mo and W, and then following the subsequent emission with a variety of x-ray diagnostics. For L-mode discharges, impurity confinement times are in the range from 17-35 ms, resulting in $D_{\rm eff}$ between 0.22 and 0.45 $m^2$/s, and the transport can be characterized as anomalous. For Ohmic plasmas, there is very little difference between impurity transport in LOC and SOC regimes, and little dependence of impurity confinement on toroidal magnetic field or background ion mass. For ICRF heated L-mode plasmas, the impurity confinement time increases

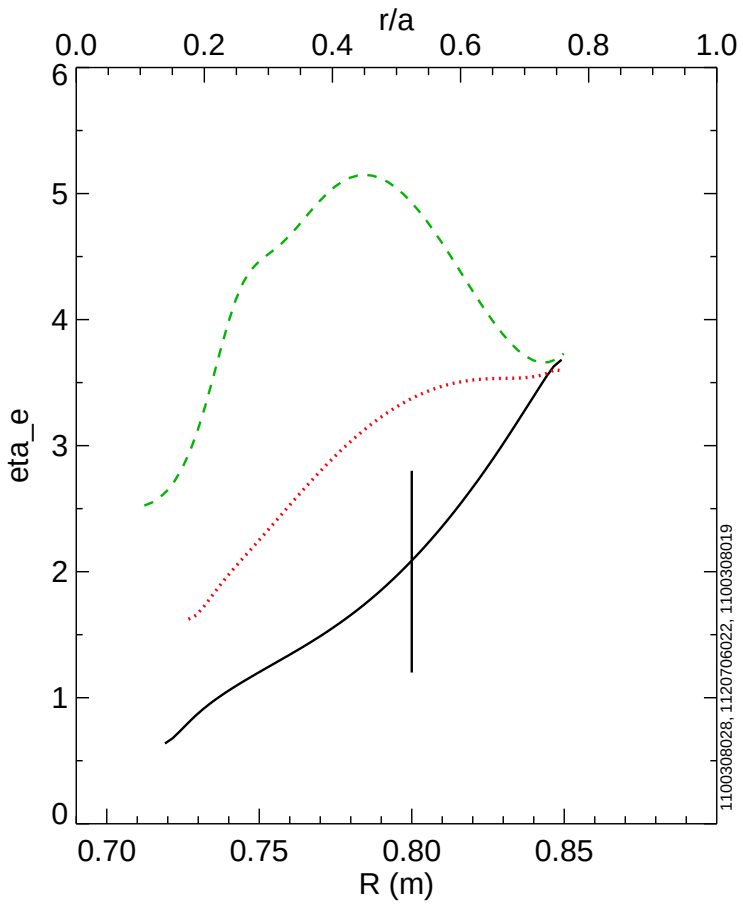


Figure 25: The spatial profiles of the ratio of the electron density to temperature gradient scale lengths for typical Ohmic L-mode (black), I-mode (dotted red) and EDA H-mode profiles (dashed green).

with plasma current and decreases with input power. The strong dependence on plasma current and weak dependence on magnetic field suggests that q is not the relevant parameter. Impurity transport in I-mode plasmas is very similar to that observed in L-mode, including the scaling with plasma current and independence on the mass of the injected impurity. Impurity confinement times in EDA H-mode plasmas are nearly an order of magnitude longer. The longer impurity confinement has been linked to the steep edge density gradient. In fact there is a strong correlation between core impurity confinement time and edge density gradient across all confinement regimes. Deduced sawtooth averaged impurity density profiles in the core are generally flat, which suggests that there is a weak impurity pinch inside of r/a $\sim 0.3$.

**VIII. Acknowledgements**

The authors thank A. Loarte, P.Diamond and C.Angioni for enlightening discussions, and the Alcator C-Mod operations and ICRF groups for expert running of the tokamak. Work supported at MIT by DoE Contract No. DE-FC02-99ER54512 and in part by an appointment to the US DOE Fusion Energy Postdoctoral Research Program administered by ORISE.

# References

[1] R.D.Petrasso *et al.*, 1986 *Phys. Rev. Lett.* **57** 707.

[2] K.Ida *et al.*, 1987 *Phys. Rev. Lett.* **58** 116.

[3] M.Kaufmann *et al.*, 1988 *Nucl. Fusion* **28** 827.

[4] G.Fussmann *et al.*, 1989 *J. Nucl. Mat.* **162-164** 14.

[5] K.Ida *et al.*, 1989 *Nucl. Fusion* **29** 231.

[6] E.J.Synakowski *et al.*, 1989 *Nucl. Fusion* **29** 311.

[7] K.W.Wenzel and D.J.Sigmar, 1990 *Nucl. Fusion* **30** 1117.

[8] M.E.Perry *et al.*, 1991 *Nucl. Fusion* **31** 1859.

[9] D.Pasini *et al.*, 1992 *Plasma Phys. Control. Fusion* **34** 677.

[10] M.Shimada, 1992 *Fusion Eng. Des.* **15** 325.

[11] J.E.Rice *et al.*, 1997 *Phys. Plasmas* **4** 1605.

[12] J.E.Rice *et al.*, 2000 *Phys. Plasmas* **7** 1825.

[13] T.Sunn Pedersen *et al.*, 2000 *Nucl. Fusion* **40** 1795.

[14] J.E.Rice *et al.*, 2002 *Nucl. Fusion* **42** 510.

[15] R.Dux *et al.*, 2003 *Plasma Phys. Control. Fusion* **45** 1815.

[16] R.Dux, 2003 *Fusion Sci. Technol.* **44** 709.

[17] M.E.Puiatti *et al.*, 2006 *Phys. Plasmas* **13** 042501.

[18] C.Giroud *et al.*, 2007 *Nucl. Fusion* **47** 313.

[19] J.E.Rice *et al.*, 2007 *Fusion Sci. Technol.* **51** 357.

[20] C.Angioni *et al.*, 2014 *Nucl. Fusion* **54** 083028.

[21] C.Angioni *et al.*, 2006 *Phys. Rev. Lett.* **96** 095003.

[22] C.Angioni *et al.*, 2007 *Phys. Plasmas* **14** 055905.

[23] C.Angioni *et al.*, 2007 *Plasma Phys. Control. Fusion* **49** 2027.

[24] C.Angioni *et al.*, 2011 *Nucl. Fusion* **51** 023006.

[25] M.Valisa *et al.*, 2011 *Nucl. Fusion* **51** 033002.

[26] M.Sertoli *et al.*, 2011 *Plasma Phys. Control. Fusion* **53** 035024.

[27] F.J.Casson *et al.*, 2013 *Nucl. Fusion* **53** 063026.

[28] E.S.Marmar *et al.*, 1980 *Phys. Rev. Lett.* **45** 2025.

[29] E.S.Marmar *et al.*, 1982 *Nucl. Fusion* **22** 1567.

[30] TFR Group, 1982 *Phys. Lett.* **87A** 169.

[31] TFR Group, 1983 *Nucl. Fusion* **23** 559.

[32] D.Pasini *et al.*, 1990 *Nucl. Fusion* **30** 2049.

[33] R.Giannella *et al.*, 1994 *Nucl. Fusion* **34** 1185.

[34] J.E.Rice *et al.*, 1995 *J. Phys. B* **28** 893.

[35] M.Mattioli *et al.*, 1995 *Nucl. Fusion* **35** 1115.

[36] J.E.Rice *et al.*, 1996 *J. Phys. B* **29** 2191.

[37] M.Mattioli *et al.*, 1998 *Nucl. Fusion* **38** 1629.

[38] E.Scavino *et al.*, 2003 *Plasma Phys. Control. Fusion* **45** 1961.

[39] N.T.Howard *et al.*, 2011 *Rev. Sci. Instrum.* **82** 033512.

[40] N.Dubuit *et al.*, 2007 *Phys. Plasmas* **14** 042301.

[41] T.Parisot *et al.*, 2008 *Plasma Phys. Control. Fusion* **50** 055010.

[42] D.Villegas *et al.*, 2010 *Phys. Rev. Lett.* **105** 035002.

[43] N.T.Howard *et al.*, 2012 *Phys. Plasmas* **19** 056110.

[44] N.T.Howard *et al.*, 2012 *Nucl. Fusion* **52** 063002.

[45] D.Villegas *et al.*, 2014 *Nucl. Fusion* **54** 073011.

[46] N.T.Howard *et al.*, 2014 *Plasma Phys. Control. Fusion* **56** xxx.

[47] R.McDermott *et al.*, 2009 *Phys. Plasmas* **16** 056103.

[48] D.G.Whyte *et al.*, 2010 *Nucl. Fusion* **50** 105005.

[49] J.E.Rice *et al.*, 2011 *Phys. Rev. Lett.* **106** 215001.

[50] A.E.Hubbard *et al.*, 2011 *Phys. Plasmas* **18** 056115.

[51] A.E.White *et al.*, 2011 *Nucl. Fusion* **51** 113005.

[52] A.E.Hubbard *et al.*, 2012 *Nucl. Fusion* **52** 114009.

[53] E.S.Marmar *et al.*, 2007 *Fusion Sci. Technol.* **51** 261.

[54] P.T.Bonoli *et al.*, 2007 *Fusion Sci. Technol.* **51** 401.

[55] J.E.Rice *et al.*, 2013 *Phys. Rev. Lett.* **111** 125003.

[56] S.M.Wolfe *et al.*, 2005 *Phys. Plasmas* **12** 056110.

[57] M.Greenwald *et al.*, 1997 *Nucl. Fusion* **37** 793.

[58] N.P.Basse *et al.*, 2007 *Fusion Sci. Technol.* **51** 476.

[59] A.Ince-Cushman *et al.*, 2008 *Rev. Sci. Instrum.* **79** 10E302.

[60] M.L.Reinke *et al.*, 2012 *Rev. Sci. Instrum.* **83** 113504.

[61] J.E.Rice *et al.*, 2014 *J. Phys. B* **47** 075701.

[62] A.Loarte *et al.*, 2014 'Tungsten impurity transport experiments in Alcator C-Mod to address high priority R&D for ITER', submitted to *Phys. Plasmas*

[63] J.E.Rice *et al.*, 1990 *Rev. Sci. Instrum.* **61** 2753.

[64] R. Mewe and J. Schrijver 1978 *Astron. Astrophys.* **65** 99.

[65] J.E.Rice *et al.*, 2011 *Nucl. Fusion* **51** 083005.

[66] J.E.Rice *et al.*, 2011 *Phys. Rev. Lett.* **107** 265001.

[67] J.E.Rice *et al.*, 2012 *Phys. Plasmas* **19** 056106.

[68] J.E.Rice *et al.*, 2013 *Nucl. Fusion* **53** 033004.

[69] S.P.Hirshman and D.J.Sigmar, 1981 *Nucl. Fusion* **21** 1079.

[70] R.J.Goldston, 1984 *Plasma Phys. Control. Fusion* **26** 87.

[71] P.N.Yushmanov *et al.*, 1990 *Nucl. Fusion* **30** 1999.

[72] C.Angioni *et al.*, 2011 *Phys. Rev. Lett.* **107** 215003.

[73] M.A.Graf *et al.*, 1995 *Rev. Sci. Instrum.* **66** 636.

[74] J.E.Rice *et al.*, 2004 *Nucl. Fusion* **44** 379.

[75] F.H.Seguin *et al.*, 1983 *Phys. Rev. Lett.* **51** 455.

[76] ITER Physics Expert Groups, 1999 *Nucl. Fusion* **39** 2175.

[77] M.Shimada *et al.*, 2007 *Nucl. Fusion* **47** S1.

[78] M.Greenwald *et al.*, 2007 *Fusion Sci. Technol.* **51** 266.

[79] J.W.Hughes *et al.*, 2013 *Nucl. Fusion* **53** 043016.

[80] J.R.Walk *et al.*, 2014 *Phys. Plasmas* **21** 056103.

[81] R.Neu *et al.*, 1997 *J. Phys. B* **30** 5057.

[82] B.LaBombard *et al.*, 2014 *Phys. Plasmas* **21** 056108.

[83] J.W.Hughes *et al.*, 2002 *Phys. Plasmas* **9** 3019.